J Mater Sci (2022) 57:526–537

Energy materials

The boosting of electrocatalytic CO_2-to-CO transformation by using the carbon nanotubes-supported PCN-222(Fe) nanoparticles composite

Lin-Wei Xu[1], She-Liang Qian[1], Bao-Xia Dong[1,*], Li-Gang Feng[1], and Zong-Wei Li[1]

[1] School of Chemistry and Chemical Engineering, Yangzhou University, Yangzhou 225002, Jiangsu, People's Republic of China

Received: 6 June 2021
Accepted: 2 October 2021
Published online: 3 January 2022

ABSTRACT

Molecular complexes with active metal centers exhibit high activity and selectivity for electrochemical CO_2 reduction reaction (CO_2RR), which represents a promising method for transforming greenhouse gas into valuable chemicals and feedstock. Using metal–organic frameworks (MOFs) to load the active molecular complexes then employing the combination with the carbonic conducting material may exhibit a beneficial effect for CO_2RR. Herein, we obtained a composite catalyst named PCN-222(Fe)/CNTs, which was in situ synthesized through the solvothermal method that loads iron porphyrin-centered PCN-222(Fe) molecules onto CNTs. The catalyst PCN-222(Fe)/CNTs exhibits excellent electrocatalytic performance for CO_2RR with a FE_{CO} of 95.5% (m(Fe-TCPP):m(CNTs) = 1:30, written as PCN-222(Fe)/CNTs-30) and an overpotential (η) of 494 mV. In addition, the turnover frequency (TOF) is high as 448.76 h^{-1} (3.011 $site^{-1}$ s^{-1}) and the hydrogen evolution reaction (HER) is indistinctive. After long-term electrocatalysis of 10 h at −0.6 V vs. RHE, PCN-222(Fe)/CNTs-30 remained its high catalytic performance with average FE_{CO} = 90%. This work provides a solid foundation for further research in the high-efficiency transformation of CO_2 to CO.

Handling Editor: Joshua Tong.

Lin-Wei Xu and She-Liang Qian authors have contributed equally to this work.

Address correspondence to E-mail: bxdong@yzu.edu.cn

https://doi.org/10.1007/s10853-021-06592-9

GRAPHICAL ABSTRACT

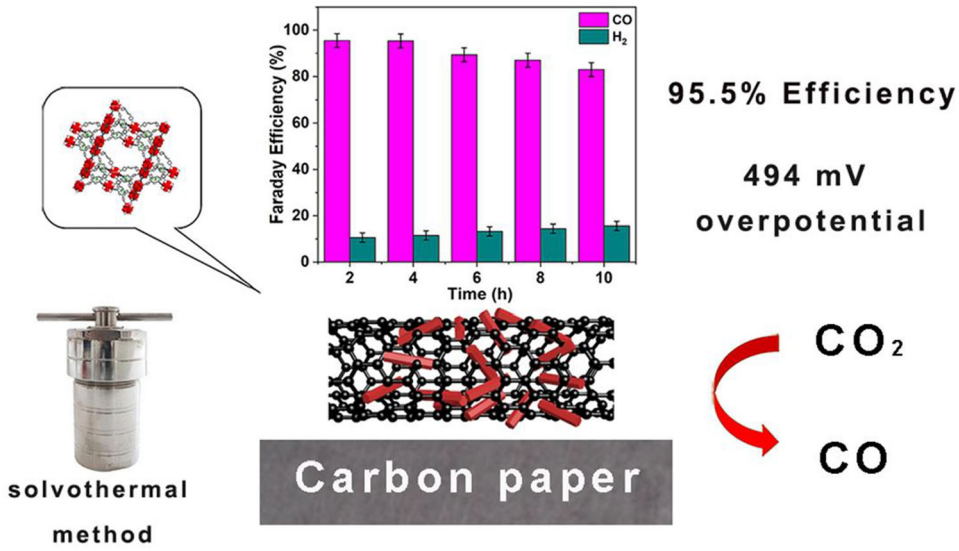

Introduction

With the continuous emission of greenhouse gases, the situation of global warming is becoming increasingly severe [1, 2]. Electrochemical CO_2 reduction reaction (CO_2RR), characterized by low energy consumption, low cost, and high conversion efficiency, is a feasible technology for transforming greenhouse gases into valuable chemicals and feedstock through renewable and clean energy sources that stands out among many methods [3–6]. Moreover, it is equally important to seek cheap and abundant materials to serve as electrocatalysts that possess excellent activity, stability, and selectivity for transforming CO_2. In this case, numerous catalysts have been developed, for instance, metal [7, 8], metallic oxide [9, 10], nonmetal material [11, 12], and heterogenous molecular complex [13, 14]. Considering the high cost and the low quantity of metal and its oxide limiting their extensive application, heteroatomic material, and molecular complex have aroused widespread interest.

Metalloporphyrin-centered molecular catalysts caught the researcher's eye because of the macrocyclic ligand framework with a conjugated structure and the regulable central metal ions with adjustable oxidation state [15, 16]. Therefore, they have been preferred in numerous redox reactions. The iron porphyrin has been reported to catalyze the CO_2 to CO electrochemically, which represented high catalytic efficiency and selectivity [17–19]. Heterogenization of the molecular catalysts is capable of further enhancing the catalytic activity, which provided more active sites with controllable chemical surroundings [20–22]. Specifically, immobilizing the iron porphyrin-related molecular catalysts onto carbonic materials has achieved remarkable results in CO_2RR. For instance, Maurin et al. [23] attached an iron molecular catalyst named CAT_{CO_2H} covalently on the CNTs, the complex of which is highly selective and active for CO_2RR in neutral water at low overpotential. Zhao et al. [24] combined Fe-porphyrin (FeTPPCl) and MWCNTs on glassy carbon electrodes, which exhibited a favorable synergistic effect and decreased overpotential of CO_2RR.

Metal–organic frameworks (MOFs), composed of inorganic metal ions/clusters and organic ligands, are porous crystalline materials that possess structural tunability, stable porosity, and adjustable functionality [25, 26]. If well modified, the composite

material is expected to exhibit the combined superiority of both the molecular catalyst and the porous architecture. For instance, Hod et al. [27] employed Fe-porphyrin-based MOFs that produced considerable catalytic sites ($\sim 10^{15}$ sites/cm^2) and 100% Faraday efficiency (FE) of the mixture of H_2 and CO. Kornienko et al. [28] employed the Al oxide rods to anchor the active TCPPCo molecules into a MOF, which revealed a FE_{CO} of 76% and a turnover number (TON) of 1400.

It is potentially beneficial for CO_2RR to employ MOFs to support the molecular catalysts (iron porphyrins) and immobilize the combination with carbonic materials. The introduction of molecular falsework makes it feasible to precisely control the spatial phase of the active catalytic centers [16]. Profiting from the flexible network structure and tunable pore surroundings, which may adsorb CO_2 to increase its concentration, the activity and selectivity of CO_2RR can be markedly promoted [29, 30]. Moreover, the addition of carbonic materials is advantageous to improve the conductivity of the catalysts, which meaning lower impedance and more effective electron transport [31, 32].

Carbon nanotubes, which are of great potential to CO_2RR, thanks to their excellent conductivity, high stability, and considerable surface area, are ideal objects for the composition of MOFs [23, 33–35]. Herein, we obtained a composite catalyst named PCN-222(Fe)/CNTs, which was in situ synthesized through the solvothermal method that loads PCN-222(Fe) molecules onto CNTs. Thereinto, PCN-222(Fe) is the MOF that is centered on iron porphyrins named Fe-TCPP (5,10,15,20-tetrakis (4-methoxycarbonylphenyl) porphyrinato]-Fe (III) chloride) (Figure S1) and extended by Zirconium oxide clusters. By virtue of different structural characterizations, it was demonstrated that the PCN-222(Fe) molecules are successfully synthesized and uniformly dispersed on the surface of the CNTs. The consequence of 2 h chronopotentiometry analysis indicated that PCN-222(Fe)/CNTs has remarkable catalytic performance for transferring CO_2 to CO with 95.5% FE_{CO} at −0.6 V vs. RHE, under a massive proportion Fe-TCPP: CNTs = 1:30. In addition, the turnover frequency (TOF) is as high as 448.76 h^{-1}, and the hydrogen evolution reaction (HER) is indistinctive.

Experimental

Preparation of materials

MWCNTs (XFNANO, 95%), DUPONT Nafion PFSA Polymer dispersions (DuPont Engineering Polymers, 99.7%), $KHCO_3$ (Aladdin, 99.5%), $FeCl_2{\cdot}4H_2O$ (Aladdin, 99%), pyrrole (Macklin, 99%), propionic acid (Macklin, 99.5%), $ZrCl_4$ (99%). *N*,*N*-dimethylformamide (99.5%), acetone (99.5%), benzoic acid (99.5%), trichloromethane (99%), tetrahydrofuran (99%), methanol (99%), methyl p-formylbenzoate (99%), and hydrochloric acid (37%) were purchased from Sinopharm Chemical reagent. The materials are all employed without refinement, and the water used was deionized in the experiments.

Synthesis of PCN-222(Fe)/CNTs

Fe-TCPP was firstly synthesized according to the method as reported [36]. The composite PCN-222(Fe)/CNTs was synthesized by a traditional one-pot solvothermal method. Specifically, we state the process by using the 1:30 portion (m(Fe-TCPP):m(CNTs) = 1:30) as an example. $ZrCl_4$ (70.0 mg), Fe-TCPP (50.0 mg), benzoic acid (2.7 g), and CNTs (1.5 g) were dissolved in DMF (8.0 mL) in a glass vial, then sealed in a reaction kettle and heated at 120 °C for 48 h. After cooling down to room temperature, the mixture was centrifuged. Afterward, 40.0 mL of DMF and 1.5 mL of HCl (8 mol L^{-1}) were added to the mixture. The reaction system was transferred to the oil bath pan and kept at 120 °C for 12 h. After cooling down, the mixture was washed with DMF and acetone twice before centrifugation and drying. The catalysts with different proportions of 1:1, 1:2, 1:3, 1:5, 1:20, and 1:40 were synthesized through a similar synthetic process except that the contents of CNTs were 50.0, 100.0, 150.0, 250.0, 1000.0, and 2000.0 mg, respectively.

Preparation of PCN-222(Fe)/CNTs electrodes

Specifically, we still state the process by using the 1:30 portion as an example. 30.0 mg of dry catalyst material was ultrasonically treated in 2.0 mL of acetone (0.5% Nafion) for 2 h to obtain a well-dispersed black slurry. The carbon paper (99.5%) was cut into 1.0 × 1.0 cm^2 pieces and pretreated overnight with 6.0 M HCl to remove residual metal impurities. The

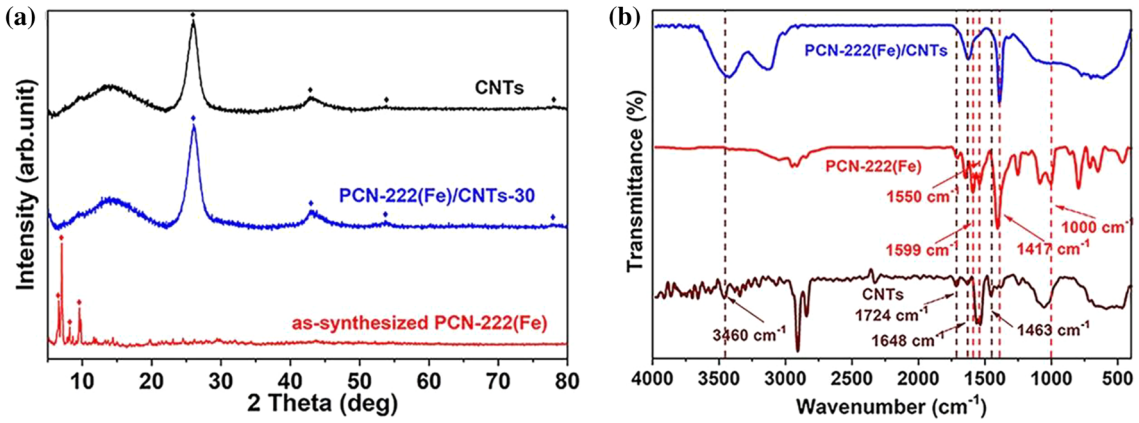

Figure 1 **a** The PXRD pattern of PCN-222(Fe), CNTs, and PCN-222(Fe)/CNTs-30. **b** The FT-IR spectra of PCN-222(Fe), CNTs, and PCN-222(Fe)/CNTs-30.

piece was then thoroughly rinsed with ultrapure water and dried before use. 40 μL slurry was dropped onto both sides of the chopped carbon paper, and the PCN-222(Fe)/CNTs electrode was obtained with a load of 3.75 mg cm^{-2}.

Results and discussion

Microstructure characterization

The catalysts at 1:1, 1:2, 1:3, 1:5, 1:20, 1:30, and 1:40 we synthesized were characterized via PXRD, FT-IR, SEM, etc., and the microstructural discussion below is focused on the PCN-222(Fe)/CNTs-30 which performed the best catalytic activity to CO_2RR. The crystalline phase of PCN-222(Fe)/CNTs at different proportions were confirmed through powder X-ray diffraction (PXRD). Figure 1a exhibits the PXRD pattern of PCN-222(Fe)/CNTs-30, pure CNTs, and the as-synthesized PCN-222(Fe). The diffraction peaks around 26.12°, 42.91°, 53.90°, and 78.04° are described as the signals of the (002), (100), (004), and (110) crystal planes of graphite [37]. Specifically, PCN-222(Fe)/CNTs-30 exhibits the characteristic peaks just as the pure CNTs, which is attributed to the coverage of the CNTs. As shown in Fig. S2a, when the load of CNTs is low, the catalysts represent favorable crystallinity of PCN-222(Fe), since the diffraction peaks appearing around 6.62°, 7.03°, 8.18°, and 9.58°, respectively, correspond to the previously reported PCN-222(Fe) [36]. With the load of CNTs increased, the characteristic peaks of PCN-222(Fe) disappear. The phenomenon demonstrates the successful combination of PCN-222(Fe) and CNTs since the diffraction peaks of the composite are in accord with CNTs and as-synthesized PCN-222(Fe).

Functional groups on CNTs, PCN-222(Fe), and PCN-222(Fe)/CNTs-30 were verified by FT-IR spectroscopy. As shown in Fig. 1b, the pattern of PCN-222(Fe)/CNTs-30 is entirely in accord with PCN-222(Fe) and CNTs. The symmetric and asymmetric stretching vibrations of carboxylic groups in PCN-222(Fe) appear at 1417 cm^{-1} and 1606 cm^{-1}, respectively. The characteristic peaks ranged in 2920–3090 cm^{-1} correspond to the C–H bond of pyrrole and benzene, and the C=C bonds of them are confirmed by the peaks around 1550–1603 cm^{-1} [38]. Moreover, the peaks of the composite at 3460 cm^{-1} and 1648 cm^{-1} are provided by CNTs. The peaks above demonstrate the successful combination of PCN-222(Fe) and CNTs. As shown in Fig. 1b and Fig. S2b, the absorption peaks of Fe–N bonds in Fe-TCPP centered at 1000 cm^{-1} are weakened to disappear [39], owing to the addition of the increasing load of CNTs, proving a successful synthesis of the composite catalyst as well.

As shown in Fig. 2, the pore size distribution and the specific surface area of PCN-222(Fe), CNTs, and PCN-222(Fe)/CNTs-30 were confirmed by N_2 adsorption–desorption tests. According to the IUPAC regulation, the isotherm of PCN-222(Fe) is classified as type I, indicating micropore structure, while a turning point at $P/P_0 = 0.3$ implies mesoporosity of PCN-222(Fe) [40]. As shown in Fig. 2d, the pores of 1.2 and 2.4 nm suggest triangular microchannels and hexagonal mesochannels, respectively, according to the density functional theory calculation (DFT).

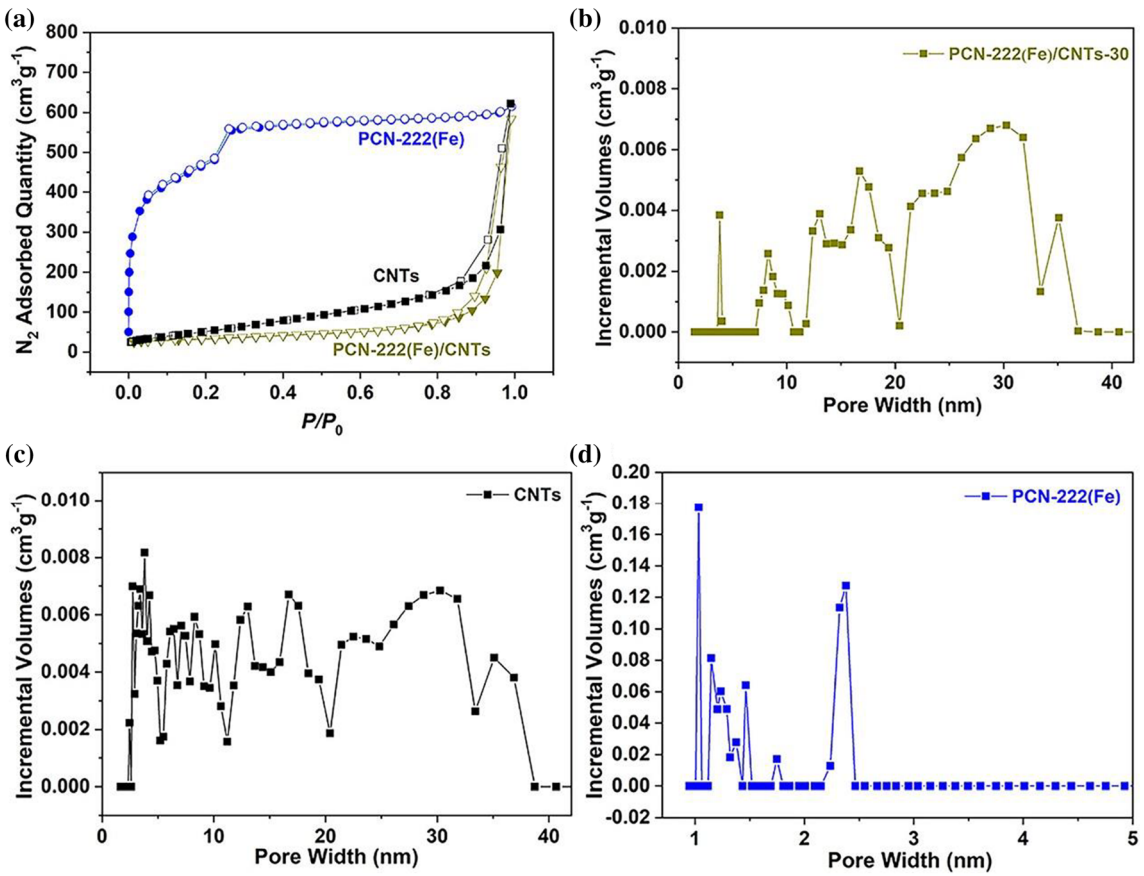

Figure 2 **a** N_2 sorption isotherms of PCN-222(Fe), CNTs, and PCN-222(Fe)/CNTs-30. **b**–**d** DFT pore size distribution of PCN-222(Fe)/CNTs-30, CNTs, and PCN-222(Fe), respectively.

However, the isotherm of PCN-222(Fe)/CNTs-30 is displayed as type IV with H3 type hysteresis loop that indicated mesopore structure [41], which can be further verified from Fig. 2c. The mesoporosity of the catalyst can be attributed to the composition of CNTs, which exhibits a type IV isotherm and mesoporosity as well. Besides, the measured BET specific surface area of the composite catalyst is 109.61 m^2 g^1, which is relatively lower than PCN-222(Fe) of 1749.01 m^2 g^{-1} but approximate to CNTs of 208.56 m^2 g^{-1} (Table S1). The discussion above demonstrates the successful combination of PCN-222(Fe) and CNTs and the mesopore structure of the composite catalyst at a ratio of 1:30.

The textural microstructure of the catalyst was illustrated by scanning electron microscopy (SEM) and transmission electron microscopy (TEM). Primitive CNTs exhibit one-dimensional fibrous morphology, and the as-synthesized PCN-222(Fe) displays a regular crystalline structure of a blocky morphology, as shown in Fig. S3. The composite PCN-222(Fe)/CNTs-30 reserves the fibrous morphology of CNTs but appears a rougher surface and a wider diameter since the CNTs are surrounded by PCN-222(Fe) (Fig. 3a, b). Furthermore, high-angle annular dark-field scanning transmission electron microscopy (HAADF–STEM) and energy-dispersive X-ray spectroscopy (EDS) were conducted to explore the surface structure of the catalyst. As shown in Fig. 3c, the composite catalyst exhibits linear morphology as displayed by TEM and SEM. Homogeneous distributions of C, N, and Fe elements can be observed on the surface of the well-defined fibrous CNTs, demonstrating a successful dispersion of PCN-222(Fe) on CNTs (Fig. 3d–f). The measurements above further confirmed the successful synthesis of the composite catalyst.

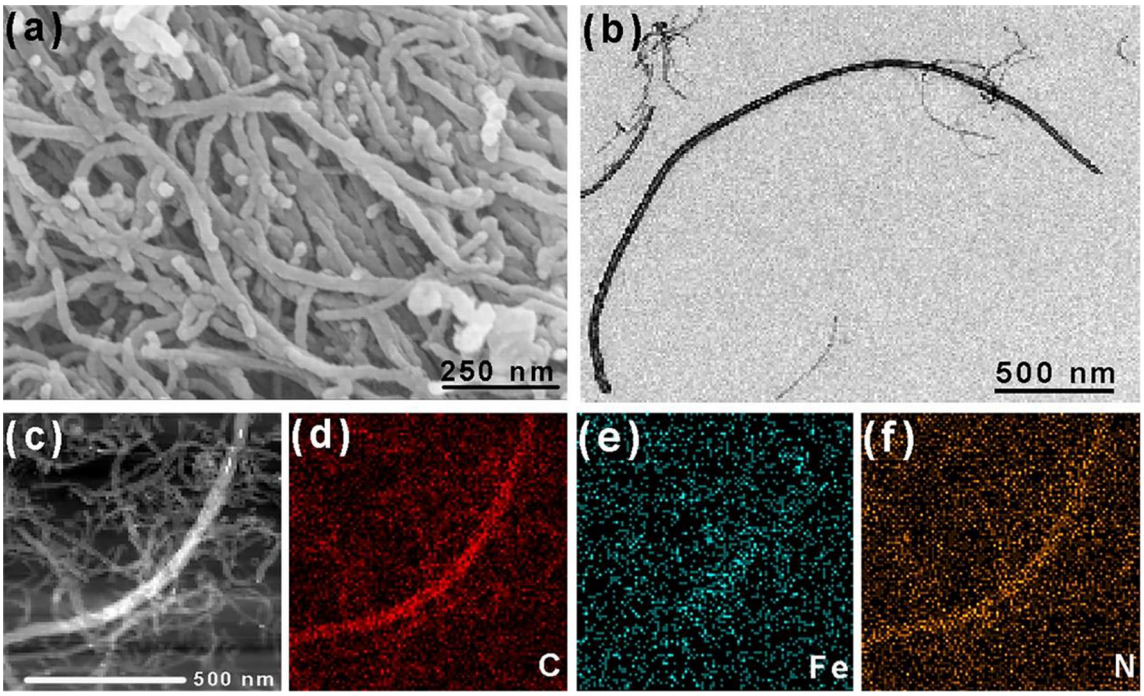

Figure 3 **a** SEM of PCN-222(Fe)/CNTs-30. **b** TEM of PCN-222(Fe)/CNTs-30. **c** HAADF–STEM of PCN-222(Fe)/CNTs-30. **d**–**f** EDS of C, N, and Fe.

Measurement of electrocatalytic performance

The catalysts were loaded on carbon paper (CP), and the optimum load of the catalysts was explored by cyclic voltammetry (CV) and potentiostatic test whose results are shown in Fig. S4. It is evident that the load of the catalyst exerts an influence on the performance of CO_2RR. Concretely, the samples with a low load of CNTs exhibit generally poor FE for CO and prominent HER (Fig. S4a–c); with a high load of CNTs at the ratio of 1:5 to 1:40, the FE for CO display maximum value varies with the loading of catalysts (Fig. S4d–g). The phenomenon is probably attributed to the fact that the increasing load of the catalysts can improve the conductivity of the electrodes but over thickened coating of the catalysts make side-effect on the conductivity and the charge transfer of the electrode. The concrete data are displayed in Table S2, and the specific calculating example is shown in Supplementary information. In the following discussion, we emphasize the optimum load of the catalysts with a higher FE_{CO} and relatively suppressed HER.

CO_2RR was conducted in a 0.5 M CO_2-saturated $KHCO_3$ aqueous solution. Figure 4a exhibits the chronoamperograms of catalysts at different proportions at −0.6 V vs. RHE. All of them show a high initial current density and reach stability after 1 h. Prior to being steady, the current density on the catalyst experienced two sections of decline and we suppose a phenomenological explanation. In section A (marked in Fig. 4a), CO_2RR didn't occur instantaneously but over a short period, and the resistance of the system was solution resistance (R_{cell}); at the end of section A, CO_2RR was activated, the resistance of the system was turned into charge transfer resistance (R_{ct}), which was much higher than R_{cell} (Table S6). The numerical variation of current density was negatively correlated to R_{ct}, which was in accord with Ohm's Law. In section B, as CO_2RR starting, numerous bubbles are generated which protrude the mass transfer process, leading to the increase in resistance and the decrease in current; Besides, being combined with CNTs decrease the excellent porosity of PCN-222(Fe), which may impede the gas transport to a certain extent. When the transportation of the gas from catalyst to solution achieved a dynamic equilibrium, the resistance of the system realized stability, resulting in an invariable current density. Gas chromatography (GC) was further employed to examine the gaseous product, and the

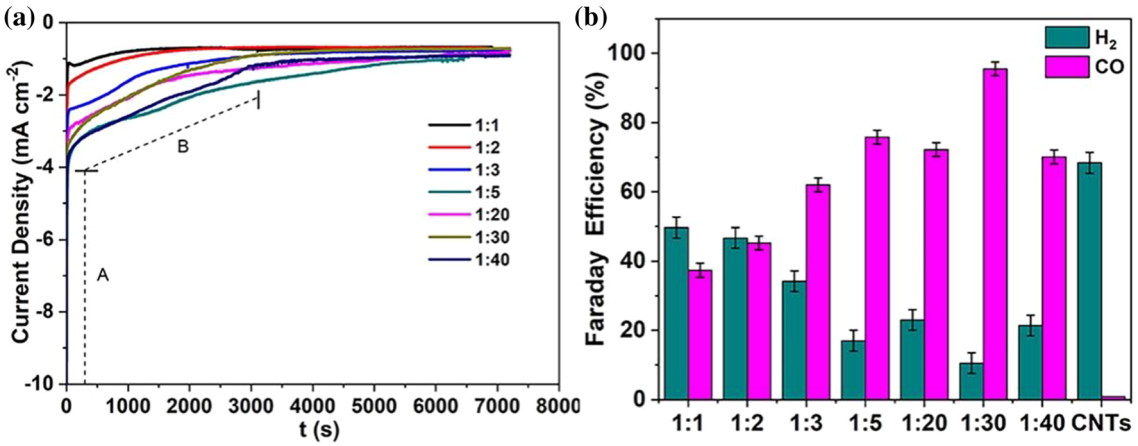

Figure 4 **a** *I–T* curve of catalysts at different ratios. **b** FE of catalysts at different ratios for CO and H_2.

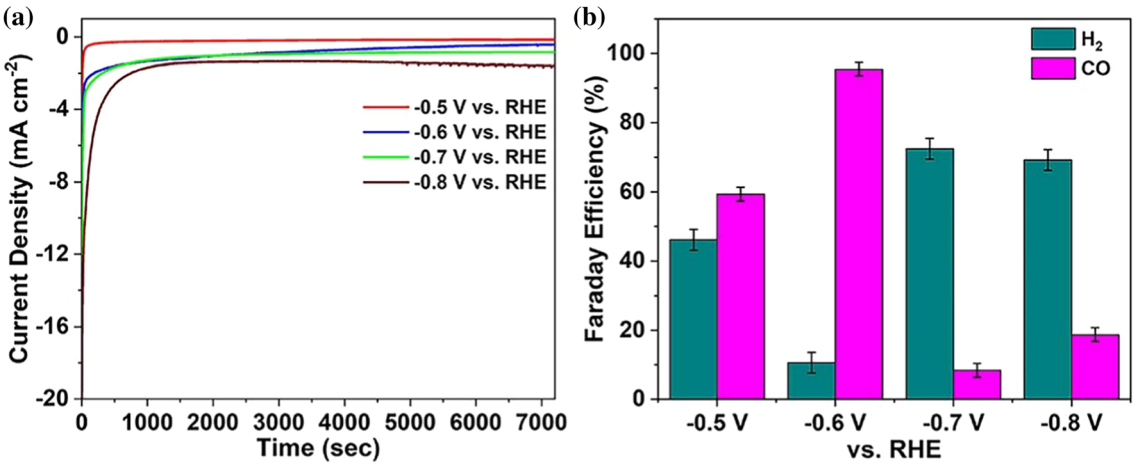

Figure 5 **a** *I–T* curve of PCN-222(Fe)/CNTs-30 at different potentials. **b** FE for CO and H_2 at different potentials.

calculation is shown in Fig. 4b. Thereinto, PCN-222(Fe)/CNTs-30 exhibits the highest FE for CO (95.5%) with 494 mV overpotential and attains a TOF of 448.76 h^{-1} (3.011 site^{-1} s^{-1}) (calculation method is elucidated in Supplementary information). For primitive CNTs, HER dominated, where the FE for H_2 is high as 70%, and the FE for CO is considerably low (less than 1%). The results above demonstrate not only excellent catalytic performance but also high selectivity of the composite catalyst. Detailed information is elucidated in Table S3.

After clarifying the conclusive role that PCN-222(Fe) played in the selectivity to CO, we explored the effect of different potentials used through the CO_2RR. Figure 5a shows the chronoamperograms of catalysts at different potentials and each of them maintains constant during the catalysis, which also exhibits short-term stability. An increase for the current density at −0.7 and −0.8 V vs. RHE are observed, and we ascribe the increase to the dominant HER [42]. Namely, the larger overpotential induces a more significant response to HER instead of CO_2RR, the consequence was further verified through the calculation of FE for H_2 and CO_2, which are plotted in Fig. 5b, and the detailed information is elucidated in Table S3. The FE for H_2 at −0.7 V vs. RHE and −0.8 V vs. RHE is approximately 70% or even more while the FE for CO is considerably low (less than 20%). At a lower potential (−0.5 V vs. RHE), there is still no improvement in the selectivity of products, which performs similar FEs for CO (59% ± 2%) and H_2 (46% ± 3%). It is safe to conclude that −0.6 V vs. RHE is the optimal potential for CO_2RR with PCN-222(Fe)/CNTs-30 served as the catalyst.

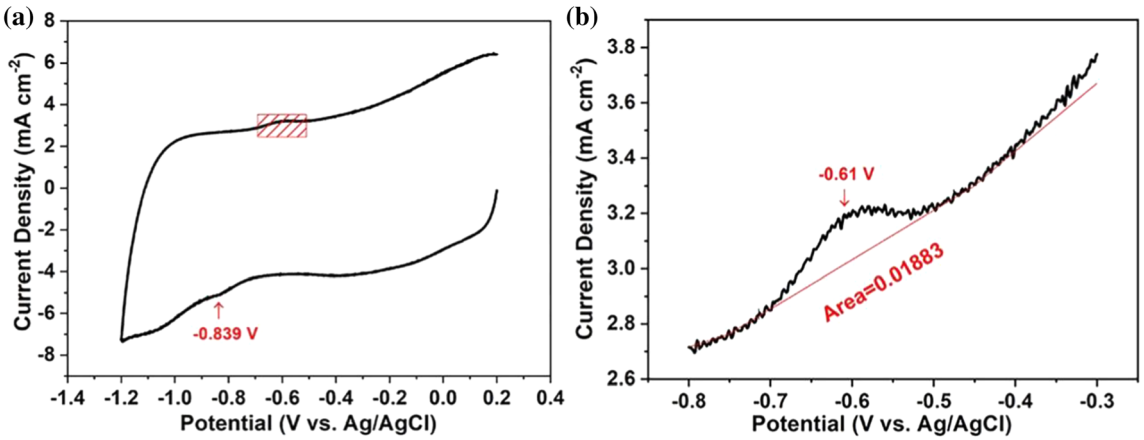

Figure 6 **a** CVs of the PCN-222(Fe)/CNTs-30, scan rate = 50 mV s^{-1}. **b** Integration of the Fe^{II}/Fe^{I} redox couple peak area.

To explore the reason for the high catalytic activity of the PCN-222(Fe)/CNTs-30, the concentration of surface electrochemically active sites (Γ) was calculated. As shown in Fig. 6a, the CV pattern of the PCN-222(Fe)/CNTs-30 exhibits one redox wave at −0.844 V vs. Ag/AgCl, which is related to the Fe^{II}/Fe^{I} redox couple [27, 43]. The electron transfer of the oxidation of Fe(I) to Fe (II) results in a peak area and the integration of which is calculated as Q_{CV} = 0.0003766 (already divided scan rate) (Fig. 6b). Γ's calculation is based on the equation: $\Gamma = Q_{CV}/nFA$ [44]. In this specific example, 'A' refers to the catalytic surface area, 'n' refers to the electron transfer of the oxidation of Fe (I) to Fe (II) (n = 1). 'F' refers to the Faraday constant. It is calculated that the Γ is 1.95×10^{-9} mol cm^{-2}. Moreover, the number of surface-active PCN-222 (Fe) sites is calculated by assuming a one-electron redox process: $n' = Q/F = 3.9 \times 10^{-9}$ mol and the surface fraction of electrochemically active PCN-222 (Fe) sites is calculated as $\chi = n'/n_{total} = 2.7\%$. More calculating details are in the Supplementary information.

ECSA (electrochemical surface area) was evaluated by the corresponding double-layer capacitance (C_{dl}) [45, 46]. The CVs of PCN-222(Fe)/CNTs loaded on CP in CO_2-saturated electrolyte (vs. Ag/AgCl) are detailed in Fig. S5. The C_{dl} values of PCN-222(Fe)/CNTs at different ratios are fitted in Fig. 7a. With the increase in the load of CNTs, the ECSA of the catalysts is promoted, which is probably attributed to the fact that as the load of CNTs increased, more active metal centers are exposed to the high conducting CNTs (Table S4). The increased ECSA facilitates rapid electron transfer and the kinetics of the electrochemical reaction [47].

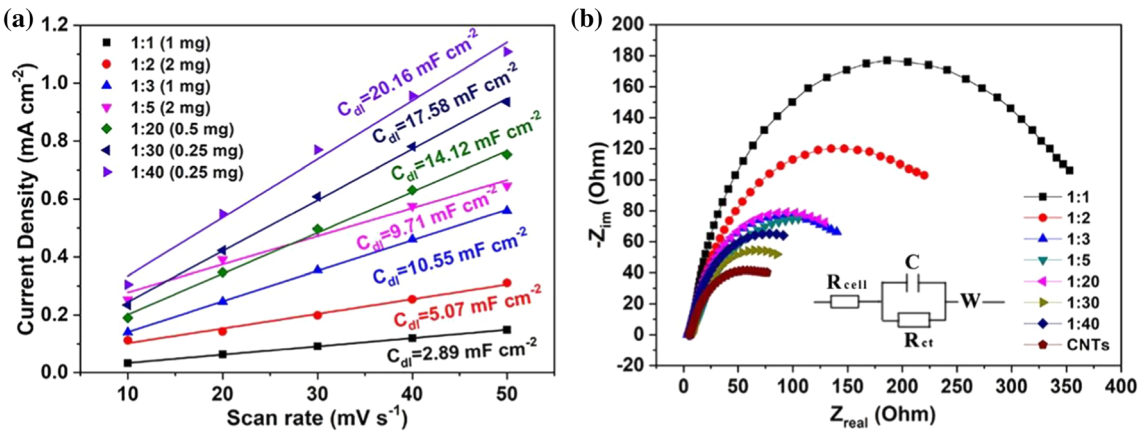

Figure 7 **a** Fitting C_{dl} values and **b** EIS of catalysts at different ratios.

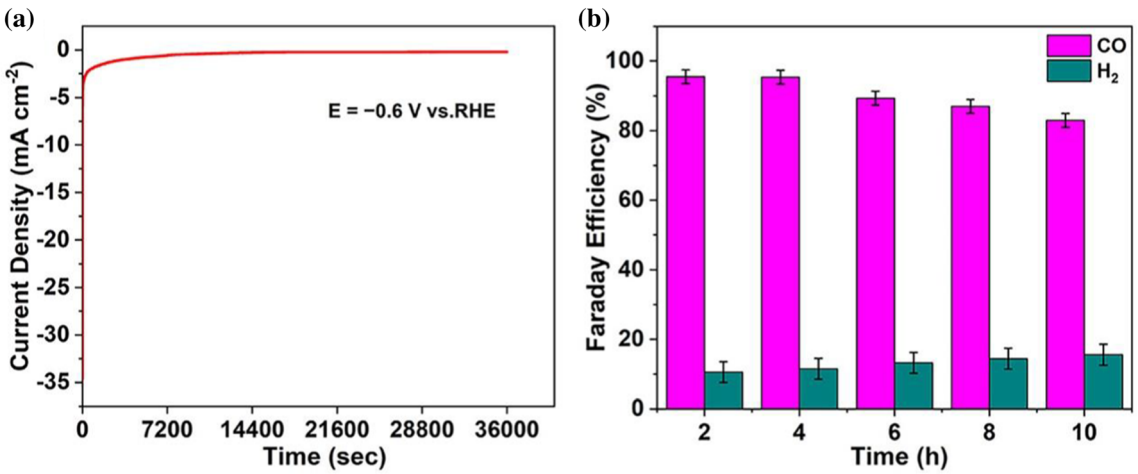

Figure 8 **a** Long-term *I–T* curve of PCN-222(Fe)/CNTs-30 and **b** FE for CO and H_2.

Moreover, to explore the influence of different CNTs contents on the conductivity of catalysts, we conducted the electrochemical impedance measurement on all samples at −1.235 V vs. Ag/AgCl. As shown in Fig. 7b, the Nyquist plots are fitted with the equivalent circuit (R_{cell}(CR_{ct})W) (inset in Fig. 7b and Table S5), which exhibits the solution resistance (R_{cell}) and the charge transfer resistance (R_{ct}) of the reaction. The R_{cell} of all samples is relatively constant, ranging from 3 to 6 Ω since the same electrolyte was employed. With the increasing load of CNTs, the radius of the semicircles accordingly declined, indicating the enhancement of the charge transferability because of the correlation of radius with R_{ct}. PCN-222(Fe)/CNTs-30 exhibits a value of 85.48 Ω, reflecting favorable electron transfer, less polarization loss, and outstanding kinetic of CO_2RR [48]. Nevertheless, when the load of CNTs is excessive, the R_{ct} increased again, which may be ascribed to an inferior synergetic effect.

Long-term chronoamperometric measurement was conducted to investigate the stability of the well-performed PCN-222(Fe)/CNTs-30 (where E = −0.6 V vs. RHE). Figure 8a shows the 10 h *i–t* curve of PCN-222(Fe)/CNTs-30, which stayed almost constant during electrocatalysis. As shown in Fig. 8b, FE for H_2 and CO are depicted. In the beginning 4 h, PCN-222(Fe)/CNTs-30 exhibits the maximum FE_{CO} of about 95.5%, and the entire electrocatalysis produced 143 μmol of CO with an average FE_{CO} of 90%, demonstrating the excellent high stability of the catalyst. The result is superior to our previous work with an average FE_{CO} of 80.4% [16]. Nevertheless, an abnormal phenomenon occurs in Fig. 8b that the total FE for CO and H_2 is higher than 100%. Considering errors in many aspects, we proposed a probable explanation in Supplementary information. Ultimately, the performance parameters of the catalyst synthesized in this work and other similar catalytic materials are compared in Table S6.

Additionally, Tafel plot was measured to explore the mechanism of the CO_2RR on the surface of the synthesized PCN-222(Fe)/CNTs [49]. Specifically in this report, FE for CO and correspond current density from −0.4 V vs. RHE to −0.6 V vs. RHE (higher potentials lose their linearity) were diffusely tested (Fig. S6a), and partial current density of CO was obtained through $j_{CO} = j \times FE(CO)$. Tafel slope was fitted by regarding lg(j_{CO}) as x-axis and overpotential (η) as y-axis with a result of 137 mV dec^{-1} (Fig. S6b), which is closed to the calculated value of about 118 mV dec^{-1} [50]. A possible CO_2RR mechanism of PCN-222(Fe)/CNTs-30 is explained in Eq. 1–4 and Eq. 2 is the possible rate-determining step (RDS), which is supported by Tafel analysis. Firstly, the dissolved CO_2 molecules are absorbed by the porous PCN-222(Fe)/CNTs-30/CP electrode (Eq. 1). Subsequently, the absorbed CO_2 molecule gets an electron and yield CO_2^-. Then in Eq. 3, the CO_2^- transfers into H_2O and CO by taking two protons and another electron. Ultimately, the absorbed CO molecule is released from the catalyst (Eq. 4).

$$CO_2\,(\text{solution}) \rightarrow CO_2\,(\text{adsorbed}) \quad (1)$$

$$CO_2\,(\text{adsorbed}) + e \rightarrow CO_2^-\,(\text{adsorbed}) \quad (2)$$

$$CO_2^-\,(\text{adsorbed}) + e + 2H^+ \rightarrow CO\,(\text{adsorbed}) + H_2O \quad (3)$$

$$CO\,(\text{adsorbed}) \rightarrow CO\,(\text{released}) \quad (4)$$

Conclusion

In general, we obtained a composite PCN-222(Fe)/CNTs catalyst through in situ solvothermal synthesis process that loads active PCN-222(Fe) molecules onto CNTs. Thanks to the favorable synergy of PCN-222(Fe) and CNTs, the catalyst PCN-222(Fe)/CNTs-30 exhibits excellent electrocatalytic performance for CO_2RR with a FE_{CO} of 95.5%, where η = 494 mV. In addition, the TOF is high as 448.76 h^{-1}, and the HER is well suppressed. The catalyst is found a high concentration of surface electrochemically active sites, a large ECSA, and a comparatively low charge transfer resistance. After long-term electrocatalysis, the catalyst exhibits high stability with an average FE_{CO} of 90%. In short, the composite catalyst PCN-222(Fe)/CNTs combines the advantages of molecular complex centered MOFs and the conducting material (CNTs). The method of combining molecular complex centered MOFs and the conducting CNTs is promising for transforming greenhouse gas into valuable chemicals and feedstock, which provides an expectation for further exploration in CO_2RR.

Acknowledgements

The authors thank the National Natural Science Foundation of China (No. 21671169), Top-notch Academic Programs Project of Jiangsu Higher Education Institutions, Six Talent Peaks Project in Jiangsu Province (No. 2017-XNY-043), and the Foundation from the Priority Academic Program Development of Jiangsu Higher Education Institutions.

Declarations

Conflict of interest The authors declare that they have no conflict of interest.

Supplementary Information: The online version contains supplementary material available at https://doi.org/10.1007/s10853-021-06592-9.

References

[1] Yu S, Yang N, Liu S, Jiang X (2021) Electrochemical and photochemical CO_2 reduction using diamond. Carbon 175:440–453. https://doi.org/10.1016/j.carbon.2021.01.116

[2] Shakun JD, Clark PU, He F, Marcott SA, Mix AC, Liu Z, Otto-Bliesner B, Schmittner A, Bard E (2012) Global warming preceded by increasing carbon dioxide concentrations during the last deglaciation. Nature 484:49–54. https://doi.org/10.1038/nature10915

[3] Yoshihara N, Arita M, Noda M (2017) Electrolyte dependence for the electrochemical CO_2 reduction activity on Cu (111) electrodes. Chem Lett 46:125–127. https://doi.org/10.1246/cl.160888

[4] Gao S, Lin Y, Jiao X, Sun Y, Luo Q, Zhang W, Li D, Yang J, Xie Y (2016) Partially oxidized atomic cobalt layers for carbon dioxide electroreduction to liquid fuel. Nature 529:68–71. https://doi.org/10.1038/nature16455

[5] Gu J, Hsu CS, Bai L, Chen HM, Hu X (2019) Atomically dispersed Fe^{3+} sites catalyze efficient CO_2 electroreduction to CO. Science 364:1091–1094. https://doi.org/10.1126/science.aaw7515

[6] Wang YR, Huang Q, He CT, Chen Y, Liu J, Shen FC, Lan YQ (2018) Oriented electron transmission in polyoxometalate−metalloporphyrin organic framework for highly selective electroreduction of CO_2. Nat Commun 9:4466–4474. https://doi.org/10.1038/s41467−018−06938−z

[7] Wang Z, Li T, Wang Q, Guan A, Cao N, Al-Enizi AM, Zhang L, Qian L, Zheng G (2020) Hydrophobically made Ag nanoclusters with enhanced performance for CO_2 aqueous electroreduction. J Power Sources 476:228705. https://doi.org/10.1016/j.jpowsour.2020.228705

[8] Gao D, Zhou H, Wang J, Miao S, Yang F, Wang G, Wang J, Bao X (2015) Size-dependent electrocatalytic reduction of CO_2 over Pd nanoparticles. J Am Chem Soc 137:4288–4291. https://doi.org/10.1021/jacs.5b00046

[9] Ohkubo K, Takahashi H, Watters EPJ, Taguchi M (2020) In-situ analysis of CO_2 electroreduction on Pt and Pt oxide cathodes. Electrochemistry 88:210–217. https://doi.org/10.5796/electrochemistry.19−00066

[10] Nellaiappan S, Sharma S (2019) Substitution of zinc (II) in nickel (II) oxide as proficient copper-free catalysts for selective CO_2 electroreduction. ACS Appl Energy Mater 2:2998–3003. https://doi.org/10.1021/acsaem.9b00242

[11] Wang H, Chen Y, Hou X, Ma C, Tan T (2016) Nitrogen-doped graphenes as efficient electrocatalysts for the selective reduction of carbon dioxide to formate in aqueous solution. Green Chem 18:3250–3256. https://doi.org/10.1039/C6GC00410E

[12] Qin Z, Jiang X, Cao Y, Dong S, Wang F, Feng L, Chen Y, Guo Y (2021) Nitrogen-doped porous carbon derived from digested sludge for electrochemical reduction of carbon dioxide to formate. Sci Total Environ 759:143575–143583. https://doi.org/10.1016/j.scitotenv.2020.143575

[13] Gu S, Marianov AN, Zhu Y, Jiang Y (2021) Cobalt porphyrin immobilized on the TiO_2 nanotube electrode for CO_2 electroreduction in aqueous solution. J Energy Chem 55:219–227. https://doi.org/10.1016/j.jechem.2020.06.067

[14] Shen J, Kortlever R, Kas R, Birdja YY, Diaz-Morales O, Kwon Y, Ledezma-Yanez I, Schouten KJP, Mul G, Koper MTM (2015) Electrocatalytic reduction of carbon dioxide to carbon monoxide and methane at an immobilized cobalt protoporphyrin. Nat Commun 6:8177–8185. https://doi.org/10.1038/ncomms9177

[15] Zhu M, Cao C, Chen J, Sun Y, Ye R, Xu J, Han YF (2019) Electronic tuning of cobalt porphyrins immobilized on nitrogen-doped graphene for CO_2 reduction. ACS Appl Energy Mater 2:2435–2440. https://doi.org/10.1021/acsaem.9b00368

[16] Dong BX, Qian SL, Bu FY, Wu YC, Feng LG, Teng YL, Liu WL, Li ZW (2018) Electrochemical reduction of CO_2 to CO by a heterogeneous catalyst of Fe-porphyrin-based metal-organic framework. ACS Appl Energy Mater 1:4662–4669. https://doi.org/10.1021/acsaem.8b00797

[17] Ambre RB, Daniel Q, Fan T, Chen H, Zhang B, Wang L, Ahlquist MSG, Duan L, Sun L (2016) Molecular engineering for efficient and selective iron porphyrin catalysts for electrochemical reduction of CO_2 to CO. Chem Commun 52:14478–14481. https://doi.org/10.1039/C6CC08099E

[18] Mondal B, Sen P, Rana A, Saha D, Das P, Dey A (2019) Reduction of CO_2 to CO by an iron porphyrin catalyst in the presence of oxygen. ACS Catal 9:3895–3899. https://doi.org/10.1021/acscatal.9b00529

[19] Costentin C, Drouet S, Robert M, Savéant JM (2012) A local proton source enhances CO_2 electroreduction to CO by a molecular Fe catalyst. Science 338:90–93. https://doi.org/10.1126/science.1224581

[20] Zhu M, Chen J, Huang L, Ye R, Xu J, Han YF (2019) Covalently grafting cobalt porphyrin onto carbon nanotubes for efficient CO_2 electroreduction. Angew Chem Int Ed 58:6595–6599. https://doi.org/10.1002/anie.201900499

[21] Manbeck GF, Fujita E (2015) A review of iron and cobalt porphyrins, phthalocyanines and related complexes for electrochemical and photochemical reduction of carbon dioxide. J Porphyr Phthalocya 19:2–20. https://doi.org/10.1142/S1088424615300013

[22] Hu XM, Rønne MH, Pedersen SU, Skrydstrup T, Daasbjerg K (2017) Enhanced catalytic activity of cobalt porphyrin in CO_2 electroreduction upon immobilization on carbon materials. Angew Chem 129:6568–6572. https://doi.org/10.1002/anie.201701104

[23] Maurin A, Robert M (2016) Catalytic CO_2-to-CO conversion in water by covalently functionalized carbon nanotubes with a molecular iron catalyst. Chem Commun 52:12084–12087. https://doi.org/10.1039/C6CC05430G

[24] Zhao HZ, Chang YY, Liu C (2013) Electrodes modified with iron porphyrin and carbon nanotubes: application to CO_2 reduction and mechanism of synergistic electrocatalysis. J Solid State Electrochem 17:1657–1664. https://doi.org/10.1007/s10008-013-2027-1

[25] Li D, Xu HQ, Jiao L, Jiang HL (2019) Metal-organic frameworks for catalysis: State of the art, challenges, and opportunities. EnergyChem 1:100005–100044. https://doi.org/10.1016/j.enchem.2019.100005

[26] Zhu L, Liu XQ, Jiang HL, Sun LB (2017) Metal−organic frameworks for heterogeneous basic catalysis. Chem Rev 117:8129–8176. https://doi.org/10.1021/acs.chemrev.7b00091

[27] Hod I, Sampson MD, Deria P, Kubiak CP, Farha OK, Hupp JT (2015) Fe-porphyrin-based metal-organic framework films as high-surface concentration, heterogeneous catalysts for electrochemical reduction of CO_2. ACS Catal 5:6302–6309. https://doi.org/10.1021/acscatal.5b01767

[28] Kornienko N, Zhao Y, Kley CS, Zhu C, Kim D, Lin S, Chang CJ, Yaghi OM, Yang P (2015) Metal-organic frameworks for electrocatalytic reduction of carbon dioxide. J Am Chem Soc 137:14129–14135. https://doi.org/10.1021/jacs.5b08212

[29] Huang X, Shen Q, Liu J, Yang N, Zhao G (2016) A CO_2 adsorption-enhanced semiconductor/metal-complex hybrid photoelectrocatalytic interface for efficient formate production. Energy Environ Sci 9:3161–3171. https://doi.org/10.1039/C6EE00968A

[30] Shen Q, Huang X, Liu J, Guo C, Zhao G (2017) Biomimetic photoelectrocatalytic conversion of greenhouse gas carbon dioxide: two-electron reduction for efficient formate production. Appl Catal B Environ 201:70–76. https://doi.org/10.1016/j.apcatb.2016.08.008

[31] Petit C, Bandosz TJ (2009) MOF-graphite oxide composites: combining the uniqueness of graphene layers and metal-organic frameworks. Adv Mater 21:4753–4757. https://doi.org/10.1002/adma.200901581

[32] Abdinejad M, Wilm LFB, Dielmann F, Kraatz HB (2021) Electroreduction of CO_2 catalyzed by nickel imidazolin-2-

ylidenamino-porphyrins in both heterogeneous and homogeneous molecular systems. ACS Sustain Chem Eng 9:521–530. https://doi.org/10.1021/acssuschemeng.0c07964

[33] Tasis D, Tagmatarchis N, Bianco A, Prato M (2006) Chemistry of carbon nanotubes. Chem Rev 106:1105–1136. https://doi.org/10.1021/cr050569o

[34] Endo M, Hayashi T, Kim YA, Muramatsu H (2006) Development and application of carbon nanotubes. Jpn J Appl Phys 45:4883–4892. https://doi.org/10.1143/JJAP.45.4883

[35] Popov VN (2004) Carbon nanotubes: properties and application. Mat Sci Eng R 43:61–102. https://doi.org/10.1016/j.mser.2003.10.001

[36] Feng D, Gu ZY, Li JR, Jiang HL, Wei Z, Zhou HC (2012) Zirconium-metalloporphyrin PCN-222: Mesoporous metal-organic frameworks with ultrahigh stability as biomimetic catalysts. Angew Chem Int Ed 51:10307–10310. https://doi.org/10.1002/anie.201204475

[37] Krajewski M, Malolepszy A, Stobinski L, Lewinska S, Slawska-Waniewska A, Tokarczyk M, Kowalski G, Borysiuk J, Wasik D (2015) Preparation and characterization of hematite-multiwall carbon nanotubes nanocomposite. J Supercond Nov Magn 28:901–904. https://doi.org/10.1007/s10948−014−2794−7

[38] Aghayan M, Mahmoudi A, Sohrabi S, Dehghanpour S, Nazaric K, Mohammadian-Tabrizi N (2019) Micellar catalysis of an iron (III)-MOF: enhanced biosensing characteristics. Anal Methods 11:3175–3187. https://doi.org/10.1039/C9AY00399A

[39] Yao B, Peng C, Zhang W, Zhang Q, Niu J, Zhao J (2015) A novel Fe (III) porphyrin-conjugated TiO_2 visible-light photocatalyst. Appl Catal B Environ 174–175:77–84. https://doi.org/10.1016/j.apcatb.2015.02.030

[40] Yu G, Song X, Zheng S, Zhao Q, Yana D, Zhao J (2018) A facile and sensitive tetrabromobisphenol-A sensor based on biomimetic catalysis of a metal-organic framework: PCN-222(Fe). Anal Methods 10:4275–4281. https://doi.org/10.1039/C8AY00831K

[41] Zhao B, Song J, Fang T, Liu P, Jiao Z, Zhang H, Jiang Y (2012) Hydrothermal method to prepare porous NiO nanosheet. Mater Lett 67:24–27. https://doi.org/10.1016/j.matlet.2011.09.057

[42] Tan X, Yu C, Zhao C, Huang H, Yao X, Han X, Guo W, Cui S, Huang H, Qiu J (2019) Restructuring of Cu_2O to Cu_2O@Cu-Metal-organic frameworks for selective electrochemical reduction of CO_2. ACS Appl Mater Interf 11:9904–9910. https://doi.org/10.1021/acsami.8b19111

[43] Maurin A, Robert M (2016) Noncovalent immobilization of a molecular iron−based electrocatalyst on carbon electrodes for selective, efficient CO_2-to-CO conversion in water. J Am Chem Soc 138:2492–2495. https://doi.org/10.1021/jacs.5b12652

[44] Lieber CM, Lewis NS (1984) Catalytic reduction of carbon dioxide at carbon electrodes modified with cobalt phthalocyanine. J Am Chem Soc 106:5033–5034. https://doi.org/10.1021/ja00329a082

[45] Simon P, Gogotsi Y (2008) Materials for electrochemical capacitors. Nat Mater 7:845–854. https://doi.org/10.1038/nmat2297

[46] Li M, Zhao Z, Cheng T, Fortunelli A, Chen CY, Yu R, Zhang Q, Gu L, Merinov BV, Lin Z (2016) Ultrafine jagged platinum nanowires enable ultrahigh mass activity for the oxygen reduction reaction. Science 354:1414–1419. https://doi.org/10.1126/science.aaf9050

[47] Zhou J, Dou Y, Zhou A, Shu L, Chen Y, Li JR (2018) Layered metal−organic framework−derived metal oxide carbon nanosheet arrays for catalyzing the oxygen evolution reaction. ACS Energy Lett 3:1655–1661. https://doi.org/10.1021/acsenergylett.8b00809

[48] Li D, Liu T, Yan Z, Zhen L, Liu J, Wu J, Feng Y (2020) MOF-derived Cu_2O/Cu nanospheres anchored in nitrogen-doped hollow porous carbon framework for increasing the selectivity and activity of electrochemical CO_2-to-formate conversion. ACS Appl Mater Interfaces 12:7030–7037. https://doi.org/10.1021/acsami.9b15685

[49] Hori Y (2008) Modern aspects of electrochemistry, vol 42. Springer, New York. doi:https://doi.org/10.1007/978-0-387-49489-0

[50] Zhang S, Kang P, Ubnoske S, Brennaman MK, Song N, House RL, Glass JT, Meyer TJ (2014) Polyethylenimine-enhanced electrocatalytic reduction of CO_2 to formate at nitrogen–doped carbon nanomaterials. J Am Chem Soc 136:7845–7848. https://doi.org/10.1021/ja5031529